Amir Bahrami* and Majid Tayarani

Chaotic Behavior of Duffing Energy Harvester

https://doi.org/10.1515/ehs-2018-0011

Abstract: A wide bandwidth energy harvester is designed with the purpose of operation under multiple excitations, where the excitation frequencies are generally incommensurate and probably spectrally close to each other. Owing this wideness of bandwidth to the nonlinearity of the circuit escalates the jeopardy of chaotic behavior while the circuit is exposed to multiple energy sources. In this study, the recently introduced Duffing based energy harvester is analyzed under multiple excitations and finally, a safe margin is calculated to avoid tumultuous behaviors which may affect adjacent sensitive electrical systems. The mathematical analyses given in this paper can be generalized to other types of nonlinear resonators.

Keywords: energy harvesting, nonlinear circuit, chaotic behavior

Introduction

Nonlinear circuits and systems have attracted a lot of attention in physics and engineering because of their versatility and multi-functionality in both their linear and nonlinear regime. The Duffing equation has played an important role in nonlinear science since many phenomena in nature with odd nonlinearity can be expressed as Duffing eq. (1). Modeling mechanical systems were just the beginning of its application; recently the Duffing equation has found its way through metamaterials (Wang et al. 2008), weak signal detection applications (Shen et al.; Li-Xin 2008), energy scavenging (Wang and Mortazawi 2015) and wireless power transfer (Wang and Mortazawi 2016). This motivated the authors to devise a mathematical approach which provides a safe margin for the behavior of the corresponding resonator under multiple excitations.

The Duffing energy harvester proposed in (Wang and Mortazawi 2016) comprises a pair of anti-series varactor diodes connected to a resistor, an inductor which models the receiving antenna inductance and a voltage source to model the received power from the environment (Figure 1). The governing equation for the corresponding circuit in terms of varactor's charge is as follows (Wang and Mortazawi 2015):

$$q'' + a_1 q + \frac{R}{L} q' + a_3 q^3 = \frac{v_1}{L}\cos(\omega_1 t) + \frac{v_2}{L}\cos(\omega_2 t) \tag{1}$$

Where a_1 and a_3 can be determined by expanding the bell-shaped C-V characteristic of anti-series varactors and are given as (Wang et al. 2008):

$$a_1 = \frac{1}{LC} = \frac{2}{LC_{jo}}, \quad a_3 = \frac{n(2n-1)}{3\ V_j^2 C_{jo}^3} \tag{2}$$

This is the general form of the damped, non-autonomous Duffing equation.

The Resonator's Behavior

The frequency response curve it tilted to the right or left for positive and negative values of a_3, respectively (Jordan and Smith 2007). As can be seen from Figure 2a, the response curve is tilted to the right because of the positive value of a_3, therefore the system is classified as hardening type (Kovacic and Brennan 2011). Depending on the direction of the frequency sweep, the resonator shows different behavior; this hysteretic behavior due to the nonlinearity can be physically interpreted by mentioning the fact that in the circuit topology given in Figure 1, no discharging path exists for varactors. The same strange behavior happens while the frequency is held constant and the input amplitude is varied as shown in Figure 2b. These amazing behaviors, although one can take advantage of, may result in chaos. Up to now, with all the explanations provided above, one may easily conclude that circuits of this kind should be designed meticulously and conservatively for both efficient and stable responses.

Figure 3 depicts the phase paths of the Duffing resonator under single-tone excitation. In Figure 3a the solution is stable since the harvester is excited by a low amplitude source. By increasing the amplitude above the chaos edge (Jin, Mei, and Li 2014), strange attractors appear in the response (Wiggins 2003). Figure 3b shows the chaotic behavior of the energy harvester under high amplitude excitation, where v is the voltage along the

***Corresponding author: Amir Bahrami,** School of electrical engineering, Iran University of Science and Technology, Tehran, Iran, E-mail: bahrami94amir@gmail.com
http://orcid.org/0000-0001-9472-4429
Majid Tayarani, School of electrical engineering, Iran University of Science and Technology, Tehran, Iran, E-mail: m_tayarani@iust.ac.ir

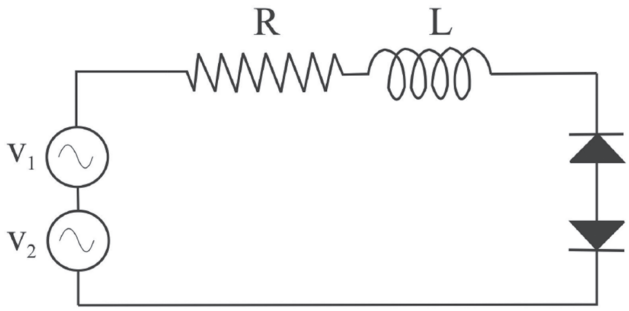

Figure 1: The equivalent circuit of Duffing energy harvester.

33-Ohm resistor and *R.q* is the charge of varactors scaled by the resistor's value. This Figure shows the phase portrait of the energy harvester scaled by the value of the resistor. In typical energy harvesting applications, neither the exact value of excitation frequency nor the exact value of excitation amplitude is of our choice, so the assurance of stability on the circuit's behavior is necessary. Here, a mathematical analysis is proposed to determine a margin for excitations which readily helps us to choose the varactors nonlinearity for both safe and efficient operation.

Mathematical Analysis

In this section, the Duffing resonator is analyzed through a familiar scenario, happening most of the times in energy scavenging applications. Consider the following scenario:

Two sources of energy, slowly approaching the harvester; in this case the exact value of excitation frequency and excitation amplitude are unknown, but we are sure that the frequencies are spectrally close and generally incommensurate, and since the energy harvester is best designed to have minimum power loss, both the damping term and excitations can be treated as perturbations. We begin our analysis using the perturbed form of eq. (1) as follow:

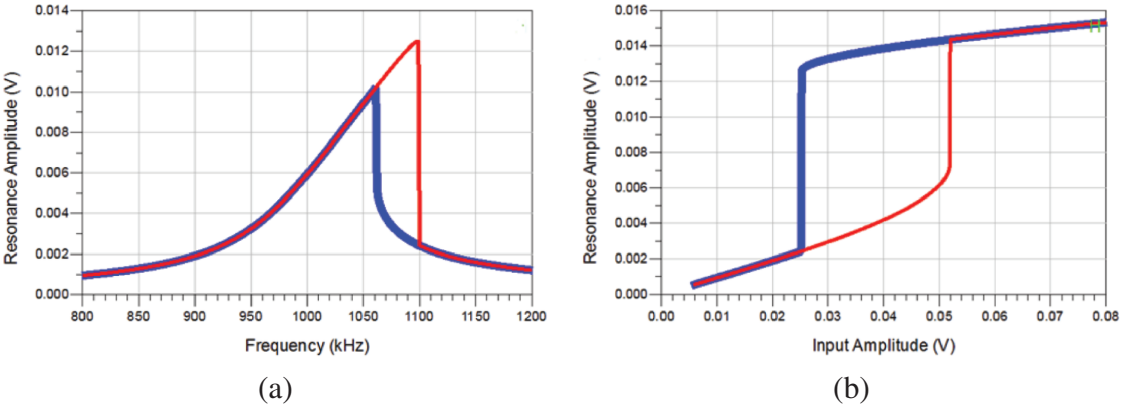

Figure 2: Single-tone circuit response for $R = 33\ \Omega$ and $\omega_0 = 1\ MHz$. Narrow-red line for forward sweep and thick-blue line for reverse sweep. (a) frequency response, (b) amplitude response.

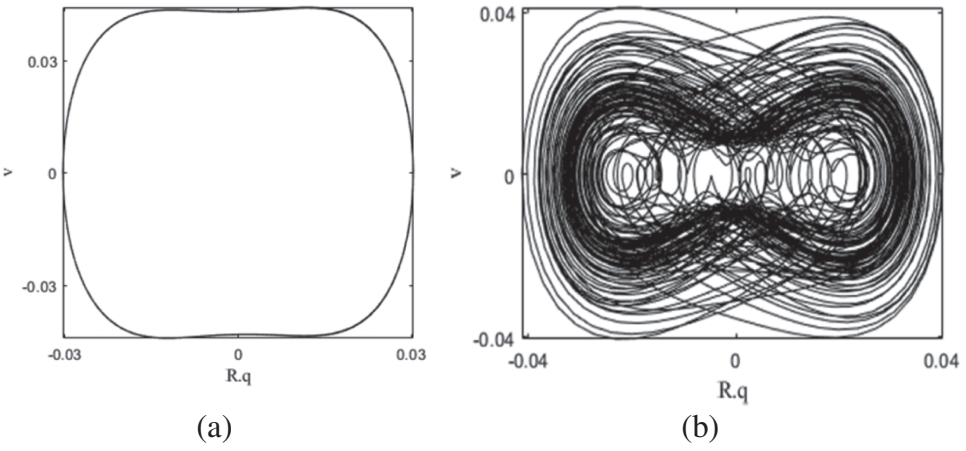

Figure 3: Phase path of Duffing energy harvester under (a) low amplitude single-tone and (b) high amplitude single tone excitation.

$$q'' + \frac{1}{LC}q = \varepsilon\left[\frac{v_1}{L}\cos(\omega_1 t) + \frac{v_2}{L}\cos(\omega_2 t) - a_3 q^3 - \frac{R}{L}q'\right] \tag{3}$$

with the following solution (Jordan and Smith 2007):

$$q = x(\tau)\cos(\omega_1 t) - y(\tau)\sin(\omega_1 t) \tag{4}$$

where x and y are slowly varying functions, modeling the behavior of the intermodulations of two excitation sources, and $\tau = \varepsilon t$ is Poincare' timescale. The averaged equation can be determined as follows (Jordan and Smith 2007):

$$\frac{dx}{d\tau} = -\frac{R}{L}x - \left[\frac{\omega_0 - \omega_1}{\varepsilon} + \frac{3a_3}{8\omega_1}r^2\right]y + \frac{v_2}{2\omega_1 L}\sin((\omega_2 - \omega_1)t) \tag{5}$$

$$\frac{dy}{d\tau} = -\frac{R}{L}x - \left[\frac{\omega_0 - \omega_1}{\varepsilon} + \frac{3a_3}{8\omega_1}r^2\right]x - \frac{v_1}{2\omega_1 L} - \frac{v_2}{2\omega_1 L}\cos((\omega_2 - \omega_1)t) \tag{6}$$

where

$$r = \sqrt{x^2 + y^2} \tag{7}$$

We apply the Melnikov's method to eqs (5) and (6), while its corresponding Hamiltonian in the absence of the resistance and second excitation is as follows:

$$V(x,y) = \frac{3a_3}{32\omega_1}r^4 + \left(\frac{\omega_2 - \omega_1}{2\varepsilon}\right)r^2 - \frac{v_1}{2\omega_1 L}x \tag{8}$$

As stated in the defined scenario the resistance and the second excitation can be considered as perturbative components. Equilibrium point of saddle type is present at $x = x_s$ and $y = 0$ where x_s is a real-valued function, minimizing the following equation:

$$x_s^3 + \frac{\omega_0 - \omega_1}{\varepsilon}x_s - \frac{4v_1}{a_3} = 0 \tag{9}$$

For the assumed value of resistance and second excitation amplitude, the eq. (5) has a closed form as:

$$x(\tau') = x_s + \frac{a_3}{16v_1}J(\tau')\left[J(\tau') + \frac{16\omega_1(\omega_1 - \omega_0)}{3a_3\varepsilon} - 2x_s^2\right]^2 \tag{10}$$

where

$$J(\tau') = -\frac{\frac{16v_1}{a_3}x_s + 2\left(\frac{8\omega_1(\omega_1 - \omega_0)}{3a_3\varepsilon} - x_s^2\right)^2}{2\sqrt{-\frac{2v_1x_s}{a_3}\cosh(\tau') - \left(\frac{8\omega_1(\omega_1 - \omega_0)}{3a_3\varepsilon} - x_s^2\right)^2}} \tag{11}$$

$$\delta^2 = -\frac{32v_1}{a_3}x_s^2 - 4\left(\frac{8\omega_1(\omega_1 - \omega_0)}{3a_3\varepsilon} - x_s^2\right)^2,\ \tau' = \frac{3\varepsilon a_3\delta(t - t_0)}{16\omega_1} \tag{12}$$

Melnikov suggests finding the distance between stable and unstable manifolds and then by finding the criterion where two manifolds intersect, the chaos criterion can be determined (Guckenheimer, Holmes, and Slemrod 1984).

The stable and unstable manifolds are as follows:

$$M_1 = \int_{-\infty}^{+\infty}\left(\left\{-\frac{R}{2L}x(\tau') + \frac{v_2}{2\omega_1 L}\sin((\omega_2 - \omega_1)t)\right\}\times \left\{(\frac{\omega_0 - \omega_1}{\varepsilon} + \frac{3a_3}{8\omega_1}r(\tau')^4)x(\tau') - \frac{v_1}{2\omega_1 L}\right\}\right)d\tau' \tag{13}$$

$$M_2 = \int_{-\infty}^{+\infty}\left(\left\{+\frac{R}{2L}y(\tau') + \frac{v_2}{2\omega_1 L}\cos((\omega_2 - \omega_1)t)\right\}\times \left\{(\frac{\omega_2 - \omega_1}{\varepsilon} + \frac{3a_3}{8\omega_1}r(\tau')^4)y(\tau')\right\}\right)d\tau' \tag{14}$$

The Melnikov function can be determined by subtracting M_1 and M_2.

$$M = \frac{R}{2L}\left\{3a_3(\frac{\mp\omega_0 \pm \omega_1}{\varepsilon})\arctan\left[\left(\frac{\theta_1 \mp \theta_2}{\theta_1 \pm \theta_2}\right)\right] - 3\delta\right\} + \frac{\pi v_2}{\omega_1 L}\mathrm{Csch}\left[\frac{16\omega_1(\omega_2 - \omega_1)}{3a_3\varepsilon}\right]\mathrm{Sin}((\omega_2 - \omega_1)t_0) \times\left\{\left(\frac{16\omega_1(\omega_2 - \omega_1)}{3a_3\varepsilon}\right)^2\frac{a_3}{16v_1}Exp\left(\mp\frac{16\omega_1(\omega_2 - \omega_1)}{3a_3\varepsilon}\arccos(\mp\frac{\theta_2}{\theta_1})\right)\right\} \tag{15}$$

where

$$\theta_1 = \sqrt{\frac{128\ v_1x_s}{a_3}};\ \theta_2 = \left(\frac{3a_3(\omega_0 - \omega_1)}{2\varepsilon\omega_1} - 4x_s^2\right) \tag{16}$$

The circuit undergoes chaotic behavior where the Melnikov function reaches zero. We are interested in the chaotic behavior of the circuit as a function of v_2 (second source of excitation); since $Sin((\omega_2 - \omega_1)t_0) < 1$ we may write the chaos criterion as follows:

$$v_2 = \frac{27v_1Ra_3}{\pi\omega_1}\left(\frac{\varepsilon a_3(\pm\omega_0 \mp \omega_1)\arctan\left[\left(\frac{\theta_1 \mp \theta_2}{\theta_1 \pm \theta_2}\right)\right] + \delta}{(\omega_2 - \omega_1)^2\mathrm{Csch}\left[\frac{16\omega_1(\omega_2 - \omega_1)}{3a_3\varepsilon}\right]}\right) \times Exp\left(\pm\frac{16\omega_1(\omega_2 - \omega_1)}{3a_3\varepsilon}\arccos(\mp\frac{\theta_2}{\theta_1})\right) \tag{17}$$

By inspecting eq. (17), one may deduce that the edge of chaos is a linear function of the resistance, showing the fact that sometimes it's better to tolerate the resistive loss than to be driven into chaos. This linear controllability over chaos unveils another application of the resonator, namely it can be used in two-tone signal sensing with variable sensitivity. Roughly speaking, the chaotic behavior exacerbates while the difference between driving frequencies is large. Figure 4 shows the phase portrait of the energy harvester for different frequencies. In this case, both excitation amplitudes are the same and the frequency of the first excitation is constant while the second excitation frequency is being varied. In Figure 4 the difference between the excitation frequencies are small, so the response is stable. By changing the second excitation frequency, quasi-periodicity appears in the output; this behavior is because of the existence of incommensurate frequencies in the output due to intermodulation products of both excitations, and though it is stable. If we keep raising the second excitation frequency up to Melnikov's criterion, the circuit undergoes chaos, as can be seen from Figure 4. In this specific application, the chaos occurrence due to the difference between frequencies of excitations is inevitable and it should be controlled by other parameters in eq. (17) such as resistance and nonlinearity of varactors.

Similar to single-tone excitation, the input amplitude can readily drive the circuit into chaos. In Figure 5 the harvester is exposed to two excitations with different frequencies. The phase portrait shows that the circuit is stable. The second amplitude of excitation is increased until the Melnikov's criterion is violated, as depicted in Figure 5, the circuit is operating in the chaotic regime.

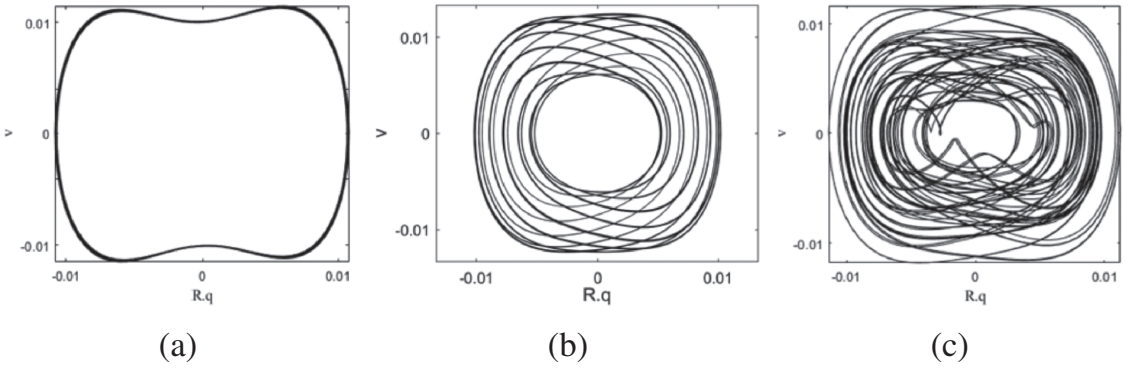

Figure 4: Phase path of Duffing energy harvester under two-tone excitation. $\omega_1 = 900$ KHz, $v_1 = v_2 = 0.01$ v and (a) $\omega_2 = 910$ KHz, (b) $\omega_2 = 1$ MHz and (c) $\omega_2 = 1.15$ MHz.

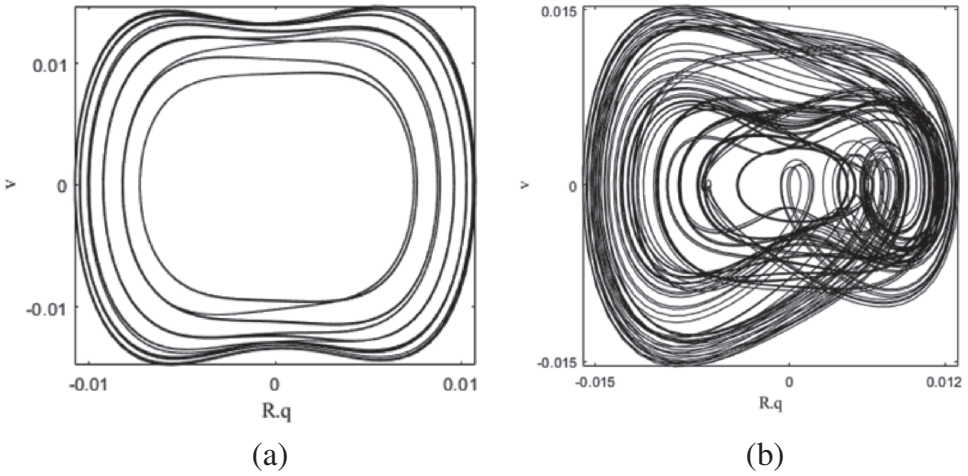

Figure 5: Phase path of Duffing energy harvester under two-tone excitation. $\omega_1 = 900$ KHz, $\omega_2 = 950$ KHz, $v_1 = 0.01$ v and (a) $v_2 = 0.009$ v and (b) $v_2 = 0.014$ v.

Table 1: Edge of chaos for various models of varactors.

y	Characteristics	Chaos Threshold
SMV1249	$n = 14, V_J = 17, C_{jo} = 39$	0.012
SMV1130	$n = 3.7, V_J = 10, C_{jo} = 25.8$	0.027
SMV1129	$n = 1.1, V_J = 2.8, C_{jo} = 27.5$	0.048

The nonlinearity of varactor diodes are key ingredients in chaos; the stronger the nonlinearity is, the more the circuit is subjected to chaos and this is an obvious fact since a strong nonlinear system tends to produce larger intermodulation products while these products are routes to chaos. Table 1 shows the chaos edge for some different models of commercially available varactors, where $\omega_2 = 1.05\ \omega_1$ and $v_1 = 0.015\ v$ and the circuit is designed to operate at $\omega_O = 1\ MHz$.

Worth mentioning that the bandwidth enhancement is only achieved when the whole circuit is driven into the nonlinear regime, so choosing an extremely weak nonlinear device, although assures the stability, cannot assure the bandwidth enhancement of the resonator.

Conclusion

In this study, a succinct but comprehensive discussion was provided on the Duffing energy harvester. Through a solid mathematical procedure, we have calculated a criterion for chaos. Therefore the chaotic behavior of such resonators can be readily controlled and we can take advantage of this chaotic behavior in other applications such as sensing. The provided procedure is not restricted to the Duffing energy harvester but it can be used for other resonators under multiple excitations and other Duffing-based systems.

References

Guckenheimer, J., P. Holmes, and M. Slemrod. 1984. "Nonlinear Oscillations Dynamical Systems, and Bifurcations of Vector Fields." *Journal Applications Mechanisms*. 184.

Jin, L., J. Mei, and L. Li. 2014. "Chaos Control of Parametric Driven Duffing Oscillators." *Applications Physical Letters* 104 (13): 104.

Jordan, D. W., and P. Smith. 2007. *Nonlinear Ordinary Differential Equations: An Introduction for Scientists and Engineers*. Keele University / OXFORD University Press.

Kovacic, I., and M. J. Brennan. 2011. *The Duffing Equation: Nonlinear Oscillators and Their Behaviour*, Hoboken, NJ, USA: John Wiley and Sons.

Li-Xin, M.. 2008. "Weak Signal Detection Based on Duffing Oscillator." In *2008 International Conference Information Managed Innov Managed Industrial Engineering*, 430–433.

Shen, L., P. Wang, W. Liu, C. Li, and J. Zhao. 2011 IEEE. *The Application of Melnikov Function in Weak Signal Detection with Duffing Oscillators*, The 2nd International Conference on Intelligent Control and Information Processing. 3–7.

Wang, B., J. Zhou, T. Koschny, and C. M. Soukoulis. 2008. "Nonlinear Properties of Split-Ring Resonators." *Optical Express* 16(20): 16058.

Wang, X., and A. Mortazawi. 2015. "Duffing Resonator Circuits for Performance Enhancement of Wireless Power Harvesters." In *2015 IEEE MTT-S International Microw Symposium IMS 2015*, 1–4.

Wang, X., and A. Mortazawi. 2016. "Bandwidth Enhancement of RF Resonators Using Duffing Nonlinear Resonance for Wireless Power Applications." *IEEE Transactions Microw Theory Technical* 64(11): 3695–3702.

Wiggins, S.. 2003. *Introduction to Applied Nonlinear Dynamical Systems and Chaos*, 2nd ed. New York: Springer-Verlag, Inc.